Journal of Colloid and Interface Science 458 (2015) 209–216

Contents lists available at ScienceDirect

Journal of Colloid and Interface Science

journal homepage: www.elsevier.com/locate/jcis

Fluorescent chemosensor for pyridine based on N-doped carbon dots

B.B. Campos [a], C. Abellán [b,c], M. Zougagh [c,d], J. Jimenez-Jimenez [e], E. Rodríguez-Castellón [e], J.C.G. Esteves da Silva [a], A. Ríos [b,c], M. Algarra [e,*]

[a] Centro de Investigação em Química, Departamento de Química, Faculdade de Ciências da Universidade do Porto, 4169-007 Porto, Portugal
[b] Department of Analytical Chemistry and Food Technology Department, University of Castilla-La Mancha, Ciudad Real, Spain
[c] Regional Institute for Applied Chemistry Research (IRICA), 13004 Ciudad Real, Spain
[d] Castilla-La Mancha Science and Technology Park, 20006 Albacete, Spain
[e] Departamento de Química Inorgánica, Facultad de Ciencias, Universidad de Málaga, Campus de Teatinos s/n, 29071 Málaga, Spain

GRAPHICAL ABSTRACT

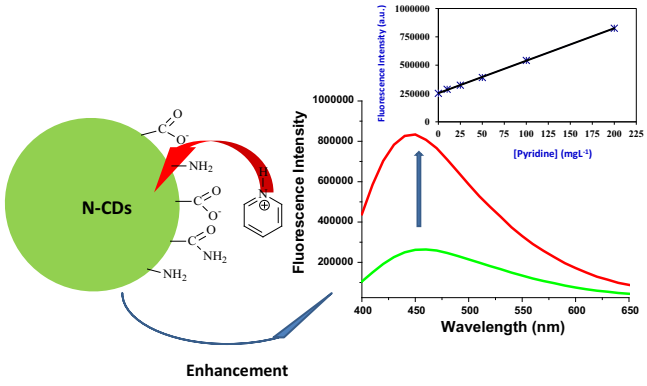

ARTICLE INFO

Article history:
Received 20 February 2015
Revised 17 July 2015
Accepted 23 July 2015
Available online 26 July 2015

Keywords:
Carbon nanomaterial
Nanoparticle
N-doped carbon dots
Pyridine sensor

ABSTRACT

Fluorescent carbon dots (CDs) and its nitrogen doped (N-CDs) nanoparticles have been synthesized from lactose as precursor using a bottom-up hydrothermal methodology. The synthesized nanoparticles have been characterized by elemental analysis, FTIR, Raman, TEM, DLS, XPS, and steady-state and life-time fluorescence. The synthesized carbon nanoparticles, CDs and N-CDs, have a size at about 7.7 ± 2.4 and 50 ± 15 nm, respectively, and quantum yields of 8% (CDs) and 11% (N-CDs). These techniques demonstrated the effectiveness of the synthesis procedure and the functionalization of the CDs surface with amine and amide groups in the presence of NH_3 in aqueous media. The effect of excitation wavelength and pH on the luminescent properties was studied. Under the optimal conditions, the nitrogen doped nanoparticles can be used as pyridine sensor in aqueous media because they show an enhancement of its fluorescence with a good linear relationship. The analytical method is simple, reproducible and very sensitive for pyridine determination.

1. Introduction

Among the recent advances of novel materials, carbon quantum dots nanoparticles (in short carbon dots, CDs), are a new class of carbonaceous nanomaterials with potential advantages to the toxic

* Corresponding author.
E-mail address: malgarra67@gmail.com (M. Algarra).

http://dx.doi.org/10.1016/j.jcis.2015.07.053
0021-9797/

metal based quantum dots (QDs). Both nanoparticles share traditional nanosized semiconductors properties, namely: size and wavelength luminescence emission dependence, resistance to photobleaching, biocompatibility associated with their nanoscale structures in conjunction with chemical functionality, among others. CDs are easily functionalized and they present some advantageous properties when they are compared to QDs [1–5].

CDs can be obtained either by chemical bottom up and/or top down synthesis methods, using different procedures. Thus, electrochemical, combustion, thermal, hydrothermal, acidic oxidation, microwave and ultrasonic, laser ablation, have been reported as techniques used for these purposes [6–19]. Although fluorescent CDs have easily been obtained by these strategies, emission features (in terms of sensitivity, meanly) and quantum yield (QY) of CDs are still scarce and highly desirable to be improved.

Doping heteroatoms into CDs has been demonstrated an effective approach to improve QY and for incorporating a surface passivation, which has showed good results [14,20]. Different strategies have been used to obtain doped CDs with nitrogen, such as those obtained by heating carbon tetrachloride and 1,2-ethylendiamine [21], by pyrolyzing ethanolamine [22], from citric acid and L-cysteine [23], glutamic [24], and folic acid [25]. The effect of different doping atoms such as N, P or B was deeply studied, as well as their influence on the photo-physical properties [26], showing that N-CDs are the most efficient [27–30].

Pyridine is an organic liquid very soluble in water [31]. It is released to the environment from industrial sources, as fugitive emissions from facilities such as coal gasification and oil shale processing [32,33]. It is used for synthesis of drugs, insecticides and herbicides [34–36]. In this way, inhalation, ingestion or skin absorption induced in humans many symptoms like headaches, infertility, respiratory distress or puke [37]. This is the reason why the determination of pyridine is very important in environmental, food and clinic fields. Some methods have been reported in the literature for the detection and quantification of pyridine, including electrostatic precipitation [38], GC [39,40], liquid chromatography–mass spectrometry (LC–MS) [41], and GC–MS [42,43].

In this article, lactose was used as precursor to develop a new method of preparing fluorescent nitrogen doped carbon dots (N-CDs) via a facile hydrothermal (solvothermal) methodology [44]. By this method, the surface of the CDs is populated by C—N organic functionalities, such as amine and amide. After exploring its chemical and physical properties, the detection capabilities of prepared N-CDs for pyridine was further exploited, revealing an enhancement of their luminescent signal, this can be used for analytical purposes.

2. Experimental

2.1. Chemicals

D-Lactose monohydrate (99%), aqueous ammonia (37%) and hydrochloric acid (37%) were purchased from Panreac SAU (Barcelona, Spain). Pyridine, anhydrous (98.8%) was purchased from Sigma–Aldrich (St. Louis, USA). Ultrapure water, used throughout all experiments, was purified through a Millipore system. All reagents were used as received without further purification.

2.2. Synthesis of doped CD nanoparticles

Raw CDs were obtained by addition of 50 mL of concentrated HCl (37%) to 50 mL of a lactose solution (1 M), followed by hydrothermally heating at 100 °C in a Teflon-equipped stainless-steel for 3 h. Finally, the remained solution was neutralized with NaOH (1 M), filtered and dialyzed against water for 24 h. The N doped CDs (N-CDs) were synthesised by following the same procedure as stated for CDs: 50 mL of aqueous NH_3 (25%) were added to 50 mL of a lactose solution (1 M), hydrothermally heated at 100 °C in a Teflon-equipped stainless-steel at 100 °C for 3 h. Finally, the remained solution was neutralised with HCl (1 M), filtered and dialyzed against water for 24 h.

2.3. Characterization methods and data analysis

The morphology was analyzed by transmission electron microscopy (TEM) and examined under a Philips CM-200 (SCAI-UMA). To obtain the size distribution histograms of CDs and N-CDs nanoparticles, it was used the Image Tool Software v_3 (UTHSCSA, USA). The zeta potential (ζ) of CDs and N-CDs were determined using a Zetasizer Nano ZS (Malvern Instruments, U.K.) equipped with a 4 mW HeNe laser operating at $\lambda = 633$ nm. The ζ measurements were also performed at 25 °C in polycarbonate folded capillary cells, incorporated with Au plated electrodes (DTS1061) and deionized H_2O was the dispersion medium. The different ζ were automatically obtained by the software, using the Stokes-Einstein and the Henry equation, with the Smoluchowski approximation. Equinox 55 FT-IR spectrometer fitted with a Golden Gate single reflection ATR accessory kit from Specac. All spectra were recorded using a resolution of 2 cm^{-1}; 50 scans were collected. The fluorescence measurements were performed with a Jovin Yvon Fluoromax 4 TCSPC (Horiba), and measured between 400 and 700 nm using an integration time of 0.1 s and 5 nm slits for excitation and emission. Resonance FT-Raman spectra, with excitation at 532 nm, were recorded on a Senterra Raman Microscope from Bruker. Fluorescence lifetime analysis was carried out using an Edinburgh Instruments FLS920, equipped with a Xe lamp (450 W) as excitation source for steady state fluorescence measurements and monochromatic LEDs (PicoQuant PLS), controlled by a PDL 880-B system. Fluorescence decays were interpreted in terms of a multi-exponential function:

$$I(t) = A + \Sigma B_i \exp^{-t/\tau_i} \quad (1)$$

where A and B_i are the pre-exponential factors and τ_i the decay times. QY of CDs and N-CDs were obtained using Rhodamine 6G as reference ($\Phi = 0.93$) in methanol ($n = 1.329$, $\lambda_{ex} = 535$ nm). The nanoparticles were dissolved in deionized H_2O_2 ($n = 1.33$) and, by using Eq. (2), QY values were obtained for both nanoparticles.

$$QY_{CDs} = QY_{st}\left[\frac{(dI/dA)_{CDs}}{(dI/dA)_{st}}\right]\left(\frac{n^2_{CDs}}{n^2_{st}}\right) \quad (2)$$

In this equation, I is the area under the fluorescence curves and A is the corresponding absorbance [45].

X-ray photoelectron spectroscopic (XPS) studies were performed by a Physical Electronic PHI 5700 spectrometer using non-monochromatic Mg Ka radiation (300 W, 15 kV, 1253.6 eV) for analyzing the core-level signals of the elements of interest with a hemispherical multichannel detector. The spectra of powdered samples were recorded with a constant pass energy value at 29.35 eV, using a 720 μm diameter circular analysis area. The X-ray photoelectron spectra obtained were analyzed using PHI ACESS ESCA-V6.0F software and processed using Multipak 8.2B package. The binding energy values were referenced to adventitious carbon C 1*s* signal (284.8 eV). Shirley-type background and Gauss–Lorentz curves were used to determine the binding energies.

2.4. DSC–TG analysis

Thermo-gravimetric analysis (TG) and differential scanning calorimetric (DSC) were performed through a TG/DSC 1 Star System (Mettler-Toledo) coupled with MS-Thermostar GSD320 (Pfeiffer Vacuum) Mass Spectrometer. TG/DSC curves were measured in Pt crucibles, in N_2 flow (20 mL/min) and using a heating rate of 5 °C min^{-1} in the range of 25–1600 °C by a HT1600 oven connected to a MX5 microbalance (thermostatic at 22 °C). The process was controlled by a STARe software v.10.0 (Mettler Toledo STARe system). All the samples were air dried in an oven at a temperature of 60 °C for one week, in order to remove the excess of water, particularly for the samples subjected to high humidity conditions.

2.5. Detection of pyridine

For the detection of pyridine by N-CDs, 5 mL of the aqueous solution of N-CDs was poured into four test tubes, which were then mixed with different volumes (50 μL, 125 μL, 250 μL, 500 μL and 1000 μL) of aqueous solution of pyridine (12.6 mM), separately. The as-produced materials were finally sonicated for 30 min and their emission fluorescence spectra were recorded (λ_{ex} = 350 nm). The concentration of pyridine was in the 0.13–2.53 mM range, where linear emission intensity – concentration relationship was found.

3. Results and discussion

3.1. Synthesis and analysis of CDs and N-CDs nanoparticles

The raw material (lactose) was selected due to its low cost and, as previously reported, because it is a source of CDs showing an excellent fluorescence signal, and presenting good surface functionalization capabilities [14,46]. Solvothermal process was chosen because allowed us to obtain a precise control over the size and shape distribution of nanoparticles [47]. Fig. 1A shows the TEM image of raw CDs, which revealed that these spherical nanoparticles were well dispersed from each other, showing a regular mean size of CDs (7.7 ± 2.4 nm). Additional TEM images are available in Fig. S1 (Supplementary information). To obtain N-CDs, the direct presence of NH_3 in the raw aqueous media was selected, instead of release it from precursors for incorporating N in the carbon matrix. N-CDs show similar spherical morphology as the CDs but with high dimensions (average diameters of 50 ± 15 nm). Also, a local nano-environment was observed around each nanoparticle, probably ascribed to the inhomogeneous thermal process (Fig. 1B).

The zeta potential of CDs and N-CDs were −7.22 and −7.58 mV, respectively, which did not change significantly after the doped process with N, and it revealed the presence of carboxylate as prominent organic groups at pH 7, as it is shown in the FTIR spectra (Fig. 2). The elemental analysis demonstrated the incorporation of N, with a N-CDs/CDs ratio of 3.9.

The FTIR spectra of CDs and N-CDs (Fig. 2) are strongly affected by the presence of H_2O, which is IR active at about 3400 and 1630 cm^{-1}, assigned to the asymmetric stretching and bending modes of O—H. Weak bands at 1431 cm^{-1} and the small shift centered at 3249 cm^{-1}, can be assigned to the presence of the stretching modes of C—N and N—H respectively, suggesting the existence of amino-containing functional groups. Apparently, N mainly exists as doping element in the core of the N-CDs, contributing to increase its QY. The absorption of the carbonyl group (C=O) at 1630 cm^{-1} is weak, due to the minor oxidation of the N-CDs in the outer surface [48], which explains the presence of the band at 1070–1030 cm^{-1}, attributed to the C—O—C stretching mode in N-CDs [49].

The 532 nm laser wavelength Raman spectra of N-CDs (Fig. 3), compared to CDs, shows a weak band at 1647 cm^{-1}, related to the vibration of sp^2 bonded carbon atoms in a two dimensional

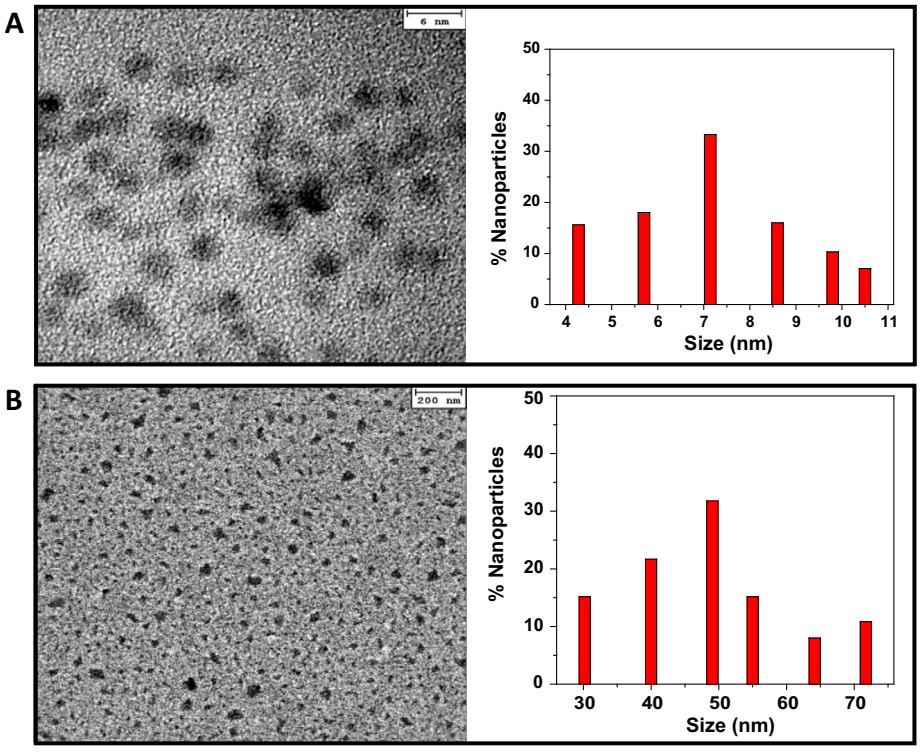

Fig. 1. TEM images of (A) CDs and (B) N-CDs nanoparticles obtained from aqueous ammonia aqueous solution (37%), showing their respective size distribution bar plots. For size distribution, 189 and 277 nanoparticles of CDs and N-CDs were analyzed, respectively.

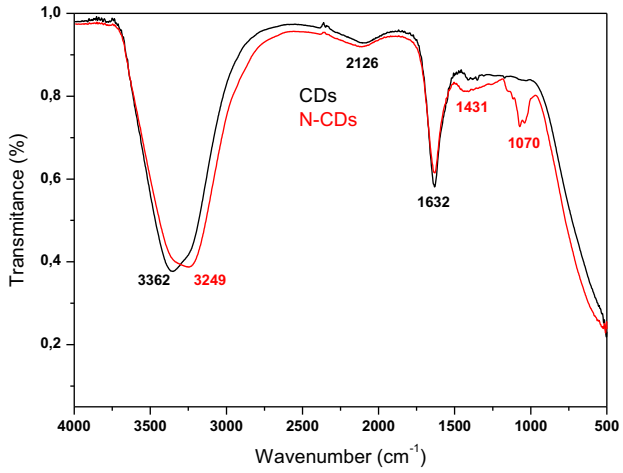

Fig. 2. FTIR spectrum of raw CDs (black) and doped N-CDs (red) nanoparticles. (For interpretation of the references to colour in this figure legend, the reader is referred to the web version of this article.)

hexagonal lattice, graphite structure. The small peak at 1350 cm^{-1} can be associated to the vibrations of carbon atoms with dangling bonds in the termination plane of disordered graphite or glassy carbon [50–52]. It is common the presence of G (1600 cm^{-1}) and D (1300–1350 cm^{-1}) bands in carbon graphitic materials; however, here a small intensity signal ascribable to the D band is detected [53]. These spectroscopic fingerprints suggest that the hydrothermal treatment reduces an important fraction of the oxygen groups of the lactose precursor, but it does not lead to a full reduction to unsaturated sp^2 species [54]. A band at 2950 cm^{-1}, observed only on disordered carbons, is suggested to be a defect-induced mode [55]. The bands centered at 3300 cm^{-1} was associated to the N—H stretch [56].

3.2. XPS analysis

The surface of the CDs and N-CDs materials were characterized by XPS. The C 1*s* core level spectrum of CDs (Fig. 4A) can be decomposed in three contributions at 284.8 eV (75%), 287.5 eV (18%) and 289.3 eV (7%). The contribution at low binding energy (284.8 eV) is the most intense and is assigned to the graphitic carbon and to adventitious carbon [51,52]. The contribution at 287.5 eV is mainly derived from the presence of carbonyl groups [52,53]; and finally,

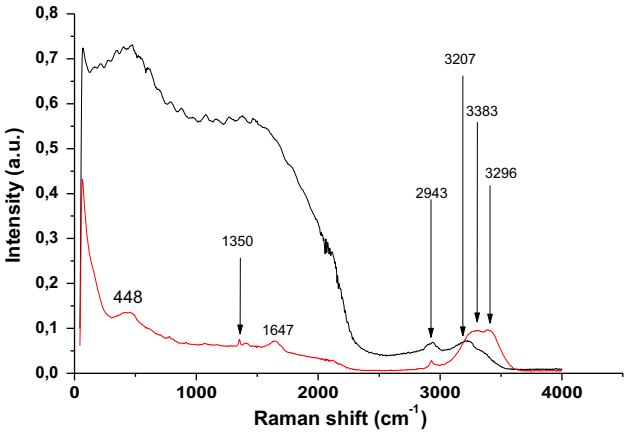

Fig. 3. Room temperature 532 FT-Raman spectrum of CDs (black) and N-CDs (red) nanoparticles. (For interpretation of the references to colour in this figure legend, the reader is referred to the web version of this article.)

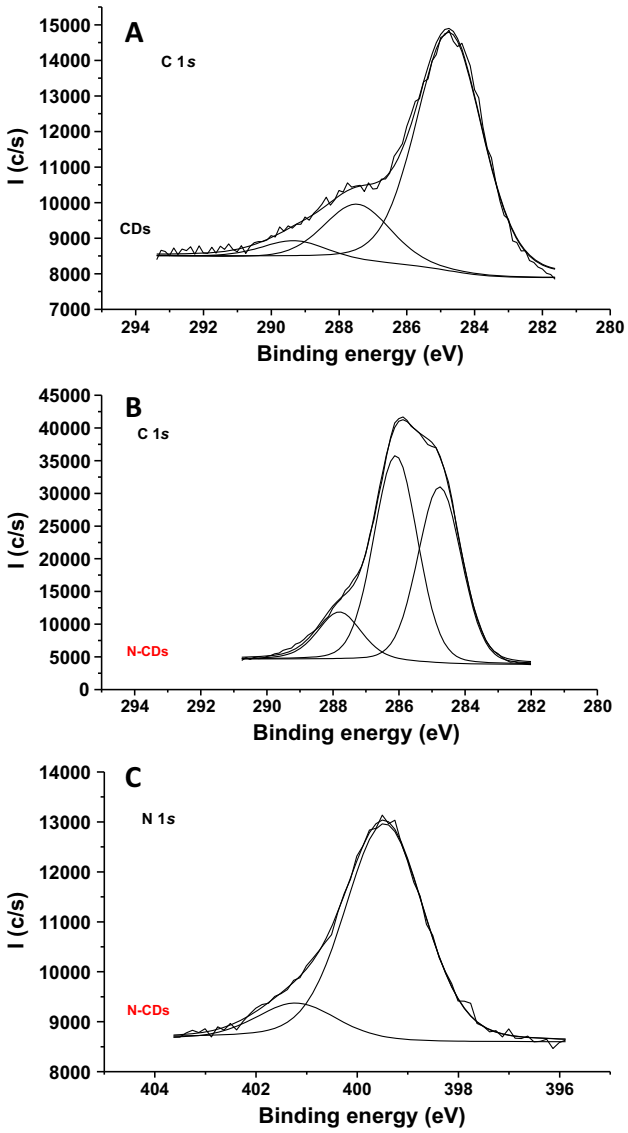

Fig. 4. (A) C 1*s* core level spectrum for sample CDs; and (B) C 1*s* and (C) N 1*s* core level spectra for sample N-CDs.

the weak contribution at 289.3 eV is due to carboxylic and carboxylate groups [51,54]. The C 1*s* core level spectrum of N-CDs can be also decomposed in three contributions at 284.8 eV (41%), 286.1 eV (47%) and 287.8 eV (12%), but showing marked differences with respect to that of CDs (Fig. 4B). Now, the contribution due to the presence of carboxylic or carboxylate groups disappears and a new contribution at 286.1 eV is more intense. This contribution is due to the presence of C—OH and C—N groups [53,54]. The N 1*s* core level spectrum is asymmetric due to the existence of two contributions at 399.5 eV (86%) and 401.2 eV (14%) (Fig. 4C). The high intensity is due to the presence of amino groups, while the contribution at high binding energy is due to the presence of NH_4^+ or alkyl ammonium groups [51,54] The atomic surface concentrations for CDs and N-CDs were C (48.05%), O (9.71%), N (0.67%), Na (21.89%), Cl (19.68%) for CDs; and C (65.72%), O (30.09%), N (3.63%) for N-CDs. The elemental analysis of the surface of N by XPS of CDs and N-CDs were 3.85% and 0.48% (in wt%), respectively. The surface mass N-CDs/CDs ratio was 7.56. This value is much higher than that observed by bulk elemental analysis (3.9), indicating that most of the N is mainly at the surface forming part of the surface nitrogen containing functionalities. The high

surface contamination with NaCl of CDs is due to the treatment with HCl and NaOH. However, N-CDs present negligible amounts of Cl and Na. In summary, XPS data show a lower atomic concentration of carbon and a higher atomic concentration of O on the surface of N-CDs, together to the appearance of N containing species mainly as amino groups, indicating that the nature of the functional groups at the surface of CDs and N-CDs are markedly different.

3.3. DTA–TG analysis

A study of the thermal stability of CDs and N-CDs was carried out in order to determine the effect of N (Fig. 5). In both cases an intense endothermic effect, associated with an important weight loss, occurs at about 100 °C, which is due to the evaporation of the water solution. In the case of pure CDs, it overlapped with other endothermic effect centered at 130 °C, both gives a weigh loss of 76% (Fig. 5A). In the case of N-CDs a weigh loss of 84% was observed until 140 °C (Fig. 5B), followed by other weigh loss of 5.20% between 300 and 500 °C, which was associated with an exothermic effect due to the combustion of the organic matter containing N. This exothermic effect was not observed in the case of CDs. These results are in agreement with those obtained by XPS and elemental analysis, demonstrating the incorporation of N containing functionalities is N-CDs. The next change is an exothermic effect which is presents in both materials, but whereas for doped N-CDs occurs at 560 °C (a weight loss of 3%), for pure CDs the exothermic effect was produced at 611 °C with a weight loss of 1%. Finally, for pure CDs a light endothermic effect, centered at 760 °C, was observed (Fig. 5A). The original files can be seen in Fig. S2 (Supplementary information).

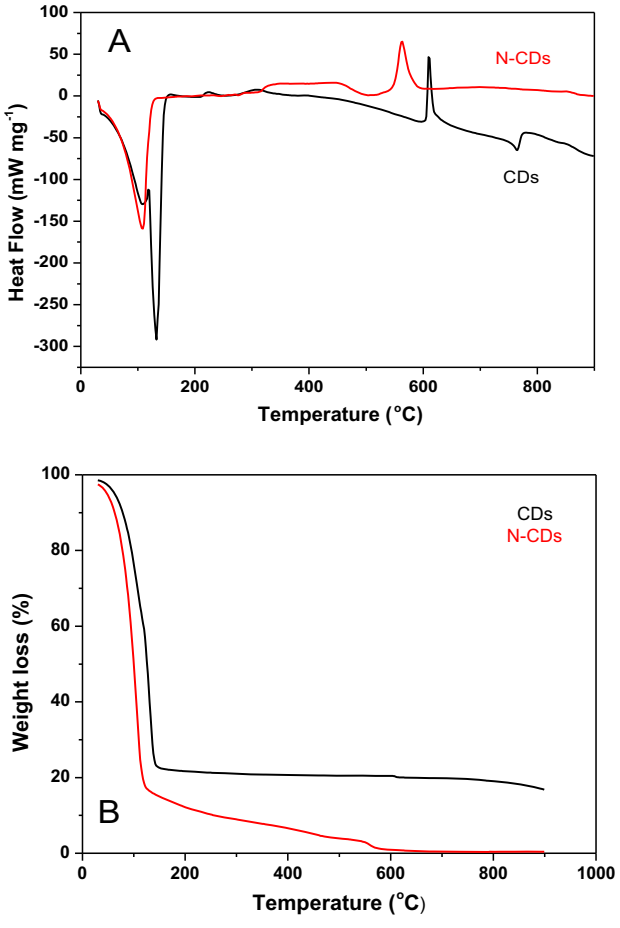

Fig. 5. (A) TG and (B) DSC curves of CDs (black) and N-CDs (red). (For interpretation of the references to colour in this figure legend, the reader is referred to the web version of this article.)

3.4. Fluorescence analysis

In order to explore the luminescent properties of N-CDs, the detailed fluorescence spectra were studied under different excitation wavelengths. As it is shown in Fig. 6, in concordance with the reported CDs and N-CDs references [46,47,55,56], the as-prepared N-CDs also exhibit a distinctive dependent fluorescent behavior. When the N-CDs were excited from 300 to 350 nm, the corresponding emission bands shifted from 440 to 460 nm. Moreover, the intensity of this emission bands were increased when the excitation wavelengths increased, showing a width at half maximum (FWHM) of 139 nm. This value indicated their size distribution dependence [57].

The highest blue emission intensity, with a QY as high as ca. 10.75%, was obtained when N-CDs were excited at 350 nm; somewhat higher compared to the raw CDs (8.10%). The observed distinctive luminescence emissions should be closely related to the N doping. The excitation-dependent fluorescent behavior of CDs can be related not only with the different sizes of N-CDs, but also from the inhomogeneous distribution of emissive sites due to the N doping [58].

The influence of pH on the fluorescence of N-CDs, in presence of pyridine, has been studied in the 1–10 pH range (Fig. 7). The presence of the N of pyridine molecule induces a change about the different signal between the signal produced by N-CDs and those produced by N-CDs in the presence of pyridine. The highest difference was observed in the pH 8–9 range, which can be explained by the presence of carboxylate ions and pyridine molecules (pK_a = 5.16). Therefore, in this range of pH, the interaction between N-CDs and pyridine is produced when the $>N^+—H$ group of pyridine interacts with the carboxylate ($—COO^-$) in the surface of N-CDs. This fact is corroborated with the values obtained of ζ, showing the negative charge susceptible of electrostatic interactions.

The measured fluorescent lifetime values for CDs and N-CDs were obtained through a two components decay time model, showing a good fit (χ^2). Although these values were expected to be sensitive to the two types of treatment, a small difference was found (Table 1). Fluorescence lifetimes for N-CDs are 2-folds than raw CDs, explained by the low excitation density, but the QY are still low. This suggests the existence of efficient non-radiative pathways involving only a single exciton. A small increase in the

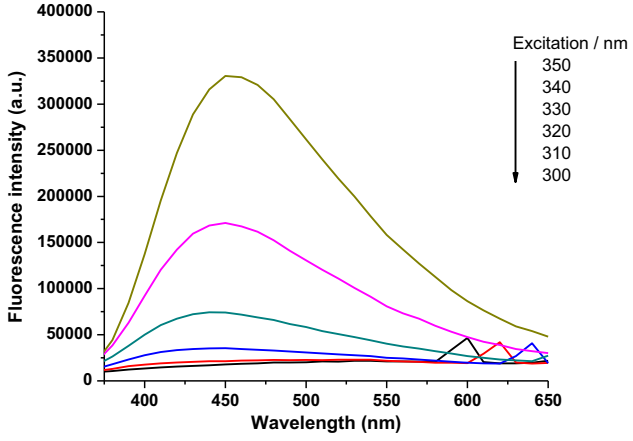

Fig. 6. Fluorescence emission spectra of N-CDs at different excitation wavelengths with at λ_{em} = 450 nm).

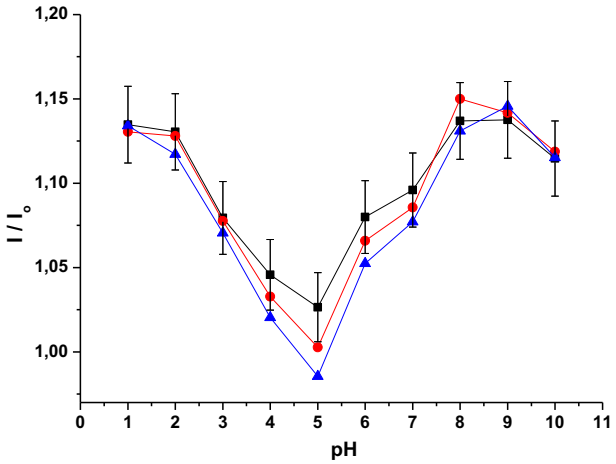

Fig. 7. Influence of pH on fluorescence intensity of N-CDs with pyridine (2×10^{-3} M) (λ_{ex} = 350; λ_{em} = 450 nm).

weight of τ_1 was observed (from 46.3% to 52.6%) in N-CDs. This is a typical behavior of a mono-exponential fitting of Eq. (1) [59].

The dilution of the N-CDs affects its fluorescence intensity. Five dilutions of N-CDs in proportions 1:25, 1:33, 1:50, 1:100, 1:200 and 1:500 with ultrapure water and PBS solution were investigated. In both cases, a 50-fold dilution was the optimum value for N-CDs. This experimental condition was considered as the stock solutions of this material because its higher fluorescence intensity. The study of the interaction of different chemical species with the surface of N-CDs is widely reported in the literature [14,15]. It has revealed that the luminescence properties of these nanomaterials strongly depend on their surface atoms and their environment [60].

3.5. Pyridine detection

In order to exploit the potential applications of the produced N-CDs, this material was directly applied in the detection of pyridine without any further functionalization. In literature, the main detection system used are based on spectrophotometric methods [61–63], where the level of detection for pyridine is at a concentration level of 0.5 mg L^{-1}. A potentiometric method was also reported for pyridine, presenting a limit of detection level of 0.28 mg L^{-1} [64]. At the same level of concentration pyridine was determined based on the quenching effect of ZnS nanoparticles coated with thioglycerol [65], or by using chitosan-CdS nano-composites films [66]. Additionally, a review of the detection systems for vapor of pyridine and related hazards can be found in the literature [67].

Therefore, the as-prepared N-CDs were evaluated as potential fluorescence probe nanosensor for pyridine. Different concentrations of an aqueous solution of pyridine were injected into the N-CDs solution and the mixture was treated under ultrasounds for 30 min before the fluorescence measurements. Fig. 8 show that the presence of pyridine induces an enhancement on the fluorescence of N-CDs, obtaining a broadness and blue shift when the concentration of pyridine increased. These modifications on the photo-physical properties on the N-CDs were produced by modifications on the surface, due to the chemical/physical sorption of pyridine molecules. The explanation of this fact can be associated to the formation of a complex, based on electrostatic interactions, when pyridine was added to the solution of N-CDs. The aggregation of nanoparticles was induced, and an energy transfer process is involved [68]. In contrast, the behavior of raw CDs when mixed with pyridine only showed small changes in the fluorescence emission spectra (see Fig. S3 in Supplementary information).

The dependence of the measured fluorescence intensity signal with increasing concentrations of pyridine was linear within the concentration range of 0.13–2.53 mM, showing a good regression

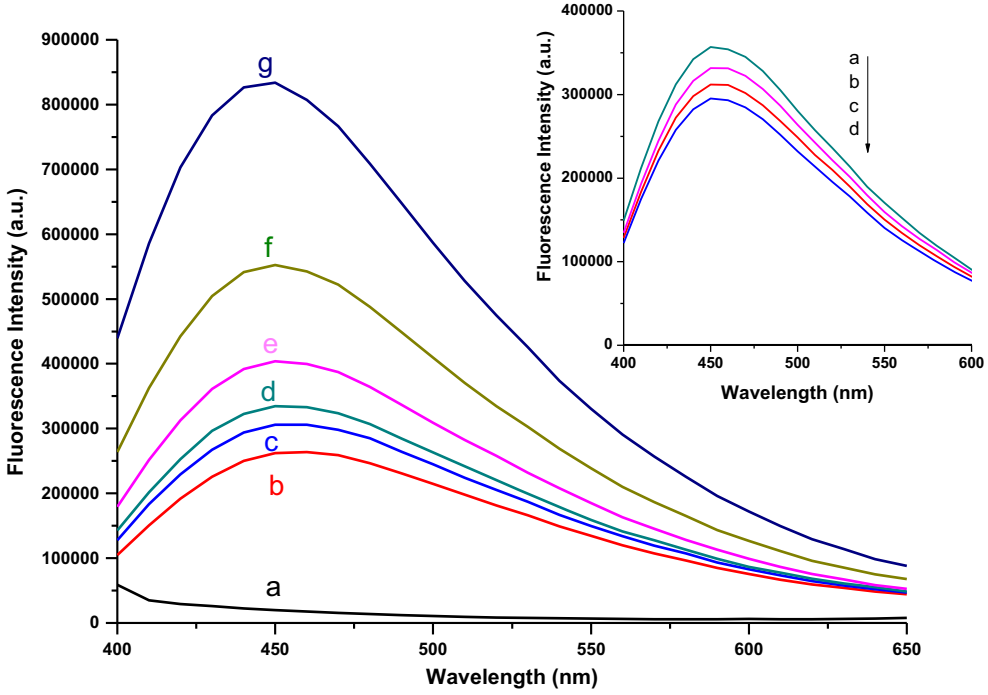

Fig. 8. Influence of pyridine concentration on fluorescence intensity of N-CDs (a) Pure pyridine; (b) Pure N-CDs; (c) 50; (d) 125; (e) 250; (f) 500 and (g) 1000 μL. Inset: Evolution of fluorescence intensity of N-CDs-pyridine (a) 5 days; (b) 3 days; (c) 3 h, and (d) Initial taken as reference (0 h); (λ_{ex} = 350; λ_{em} = 450 nm).

Table 1
Fluorescence lifetime CDs and N-CDs obtained from lactose.

	A	B_1	B_2	τ_1 (ns)	τ_2 (ns)	χ^2
CDs	16.914	0.0247	0.0068	1.045 (46.3%)	4.395 (53.7%)	1.089
N-CDs	49.401	0.0580	0.0134	2.265 (52.6%)	8.824 (47.4%)	1.084

A and B_i are the pre-exponential factor.
τ_i the lifetimes.

Table 2
Calibration data and validation parameters obtained for pyridine determination by using the proposed fluorescence chemosensor.

Linear range (mM)	0.13–2.53
Intercept ($a \pm S_a$) $\times 10^4$	2505.6 ± 0.1
Slope ($b \pm S_b$) $\times 10^4$	22.8 ± 0.1
R^2	0.9999
$S_{y/x}$	2.6×10^3
LOD (mM)	0.03
LOQ (mM)	0.11
RSD	0.25

a: Intercept; S_a: SD of the intercept; b: slope; S_b: SD of the slope; R: regression coefficient; $S_{y/x}$: SD of residuals; RSD: relative standard deviation ($n = 10$).

coefficient ($R^2 = 0.999$). The figures of merit of the method are summarized in Table 2. The LOD obtained was 0.03 mM, which presents advantages with respect to the previous value using other similar fluorescent sensor for detection of pyridine, for which a LOD of 0.068 mM was reported [69]. Moreover, in addition to the good sensitivity, with the sensor proposed here, very reproducible results were obtained, involving a simple methodology at much reduced costs. The precision, expressed in terms of relative standard deviation (RSD), was 0.25% ($n = 10$), which are at the level order of concentration of the previous analytical methods described.

4. Conclusions

In conclusion, we have presented a facile and rapid method to obtain N-CDs by using lactose as the precursor under a solvothermal process, under the treatment with NH_3 at 100 °C. The as-prepared N-CDs, with spherical morphology and a distribution of nanoparticles with an 3×10^{-5} average diameter of 50 ± 15 nm (lager than the un-treated with NH_3, 7.7 ± 2.4 nm). N-CDs showed a moderate quantum yield (10.75%) and bright green fluorescence. By XPS and Raman spectroscopy it was elucidated the presence of surface carbonyl, amine and amide functional groups. Also, N-CDs showed sensitivity towards pyridine in aqueous media because it enhanced the fluorescence of N-CDs proportionally to the concentration, being its limit of detection of 0.03 mM with a precision of 0.25%, while raw CDs did not show outstanding change on the fluorescence intensity when mixed with pyridine. The method is simple, sensitive and a low cost is involved.

Acknowledgments

M. Algarra is gratefully to the PLASMON program from ESF for the Exchange Grant. B.B Campos is gratefully to Grant SFRH/BD/84318/2012 to FCT (Lisbon, Portugal) Financial support from the Spanish Ministry of Economy and Competitiveness (CTQ2013-48411-P) and Junta Comunidades Castilla-La Mancha (Project PEIC-2014-001-P) are gratefully acknowledged. The support given through an "INCRECYT" research contract to M. Zougagh is also acknowledged.

Appendix A. Supplementary material

Supplementary data associated with this article can be found, in the online version, at http://dx.doi.org/10.1016/j.jcis.2015.07.053.

References

[1] Y.P. Sun, B. Zhou, Y. Lin, W. Wang, K.A.S. Fernando, P. Pathak, M.J. Meziani, B.A. Harruff, X. Wang, H. Wang, P.G. Luo, H. Yang, M.E. Kose, B. Chen, L.M. Veca, S.Y. Xie, J. Am. Chem. Soc. 128 (2006) 7756.
[2] S.N. Baker, G.A. Baker, Angew. Chem. Int. Ed. 49 (2010) 6726.
[3] Q. Liang, W. Ma, Y. Shi, Z. Li, X. Yang, Carbon 60 (2013) 421.
[4] S. Zhu, Q. Meng, L. Wang, J. Zhang, Y. Song, H. Jin, K. Zhang, H. Sun, H. Wang, B. Yang, Angew. Chem. Int. Ed. 52 (2013) 3953.
[5] Y. Wang, A. Hu, J. Mater. Chem. C 2 (2014) 6921.
[6] H.T. Li, X.D. He, Z.H. Kang, H. Huang, Y. Liu, J.L. Liu, S.Y. Lian, C.H.A. Tsang, X.B. Yang, S.T. Lee, Angew. Chem. Int. Ed. 49 (2010) 4430.
[7] H. Ming, Z. Ma, Y. Liu, K.M. Pan, H. Yu, F. Wang, Z.H. Kang, Dalton Trans. 41 (2012) 9526.
[8] J.G. Zhou, C. Booker, R.Y. Li, X.T. Zhou, T.K. Sham, X.L. Sun, Z.F. Ding, J. Am. Chem. Soc. 129 (2007) 744.
[9] Z.L. Wu, P. Zhang, M.X. Gao, C.F. Liu, W. Wang, F. Leng, C.Z. Huang, J. Mater. Chem. B 1 (2013) 2868.
[10] Z. Yang, Z. Li, M. Xu, Y. Ma, J. Zhang, Y. Su, F. Gao, H. Wei, L. Zhang, Nano-Micro Lett. 5 (2013) 247.
[11] C.Z. Zhu, J.F. Zhai, S.J. Dong, Chem. Commun. 48 (2012) 9367.
[12] X.Y. Qin, W.B. Lu, A.M. Asiri, A.O. Al-Youbi, X.P. Sun, Catal. Sci. Technol. 3 (2013) 1027.
[13] S. Sahu, B. Behera, T.K. Maiti, S. Mohapatra, Chem. Commun. 48 (2012) 8835.
[14] M. Algarra, B.B. Campos, K. Radotić, D. Mutavdžić, T.J. Bandosz, J. Jiménez-Jiménez, E. Rodriguez-Castellon, J.C.G. Esteves da Silva, J. Mater. Chem. A 2 (2014) 8342.
[15] M. Algarra, M. Pérez-Martín, M. Cifuentes-Rueda, J. Jiménez-Jiménez, J.C.G. Esteves da Silva, T.J. Bandosz, E. Rodríguez-Castellón, J.T. López-Navarrete, J. Casado, Nanoscale 6 (2014) 9071.
[16] H. Li, X. He, Y. Liu, H. Huang, S. Lian, S.T. Lee, Z. Kang, Carbon 49 (2011) 605.
[17] X. Wang, L. Cao, F.S. Lu, M.J. Meziani, H. Li, G. Qi, B. Zhou, B.A. Harruff, F. Kermarrec, Y.P. Sun, Chem. Commun. (2009) 3774.
[18] G.X. Chen, M.H. Hong, T.C. Chong, H.I. Elim, G.H. Ma, W. Ji, J. Appl. Phys. 95 (2004) 1455.
[19] H. Gonçalves, P.A.S. Jorge, J.R.A. Fernandes, J.C.G. Esteves da Silva, Sens. Act. B Chem. 145 (2010) 702.
[20] A. Sachev, I. Matai, P. Gopinath, RSC Adv. 4 (2014) 20915.
[21] S. Liu, J. Tian, L. Wang, Y. Luo, J. Zhai, X. Sun, J. Mat. Chem. 21 (2011) 11726.
[22] X. Dong, Y. Su, H. Geng, Z. Li, C. Yang, X. Li, Y. Zhang, J. Mater. Chem. C 2 (2014) 7477.
[23] Y. Dong, H. Pang, H.B. Yang, C. Guo, J. Shao, Y. Chi, C.M. Li, T. Yu, Angew. Chem. Int. Ed. 52 (2013) 7800.
[24] J. Niu, H. Gao, J. Luminescence 149 (2014) 159–162.
[25] M.K. Barman, B. Jana, S. Bhattacharyya, A. Patra, J. Phys. Chem. C. 118 (2014) 20034.
[26] W. Guan, W. Gu, L. Ye, C. Gui, s. Su, P. Xu, M. Xue, Int. J. Nanomedicine 9 (2014) 5071.
[27] G. Xu, G. He, Z. Li, F. He, F. Gao, Y. Su, L. Zhang, Z. Yang, Y. Zhang, Nanoscale 6 (2014) 10307.
[28] G. Jiang, T. Jiang, X. Li, Z. Wei, X. Du, X. Wan, Mater. Res. Express 1 (2014) 025708.
[29] Y.Q. Zhang, D.K. Ma, Y. Zhuang, X. Zhang, W. Chen, L.L. Hong, Q.X. Yan, K. Yu, S.M. Huang, J. Mater. Chem. 22 (2012) 16714.
[30] Y.Q. Zhang, D.K. Ma, Y.G. Zhang, W. Chen, S.M. Huang, Nano Energy 2 (2013) 545.
[31] D.R. Lide (Ed.), Handbook of Chemistry and Physics (nineteenth ed.), Boca Raton, CRC Press, 2009.
[32] G.K. Sims, E.J. O'Loughlin, R.L. Crawford, Crit. Rev. Environ. Contr. 19 (1989) 309.
[33] D.H. Stuermer, D.J. Ng, C.J. Morris, Environ. Sci. Tech. 16 (1982) 582.
[34] J.A. Joule, K. Mills, Heterocyclic Chemistry, fifth ed., Blackwell Publishing, Chichester, 2010.
[35] S. Shimizu, N. Watanabe, T. Kataoka, T. Shoji, N. Abe, S. Morishita, H. Ichimura, Pyridine and Pyridine Derivatives, Ullmann's Encyclopedia of Industrial Chemistry, 2002.
[36] E.A. Bakhite, A.A. Abd-Ella, m.E. El-Sayed, S.A. Abdel-Raheem, J. Agric. Food Chem. 62 (2014) 9982.
[37] International Agency for Research on Cancer (IARC), "Pyridine Summary & Evaluation", IARC Summaries & Evaluations, IPCS INCHEM, 2007.
[38] E.L. White, M.S. Uhrig, T.J. Johnson, B.M. Gordon, R.D. Hicks, M.F. Borgerding, W.M. Coleman III, J.F. Elder Jr., J. Chromatogr. Sci. 28 (1990) 393.
[39] H. Tang, G. Richards, K. Gunter, J. Crawford, M.L. Lee, E.A. Lewis, D.J. Eatough, J. High Resolut. Chromatogr. Chromatogr. Commun. 11 (1988) 775.
[40] K.D. Brunnemann, G. Stahnke, D. Hoffmann, Anal. Lett. 11 (1978) 545.
[41] S. Saha, R. Mistri, B.C. Ray, J. Chromatogr. A 1217 (2010) 307.
[42] S. Vainiotalo, R. Vaaranrinta, J. Tornaeus, N. Aremo, T. Hase, K. Peltonen, Environ. Sci. Technol. 35 (2001) 1818.

[43] G. Pieraccini, S. Furlanetto, S. Orlandini, G. Bartolucci, I. Giannini, S. Pinzauti, G. Moneti, J. Chromatogr. A 1180 (2008) 138.
[44] M. Choucair, P. Thordarson, J.A. Stride, Nat. Nanotech. 4 (2008).
[45] A.M. Brouwer, Pure Appl. Chem. 83 (2011) 2228.
[46] C. López, M. Zougagh, M. Algarra, E. Rodríguez-Castellón, B.B. Campos, Joaquim C.G. Esteves da Silva, J. Jiménez-Jiménez, A. Ríos, Talanta 132 (2015) 845.
[47] S.L. Hu, K.Y. Niu, J. Sun, J. Yang, N.Q. Zhao, X.W. Du, J. Mater. Chem. 19 (2009) 484.
[48] R. Vikneswaran, S. Ramesh, R. Yahya, Mat. Lett. 136 (2014) 179.
[49] B. Wang, Y. Zhang, Z. Guo, J. Cheng, Z. Fang, J. Polym. Res. 18 (2011) 187.
[50] S. Iijima, Nature 354 (1991) 56.
[51] Z.H. Kang, E.B. Wang, S.Y. Lian, L. Gao, M. Jiang, C.W. Hu, L. Xu, Nanotechnology 15 (2004) 490.
[52] M.S. Dresselhaus, G. Dresselhaus, M.A. Pimenta, P.C. Eklund, in: M. J. Pelletier (Ed.), Analytical Applications of Raman Spectroscopy, Blackwell Science, Oxford, 1999, (Chap. 9).
[53] G. Gouadec, P. Colomban, Prog. Cryst. Growth Charact. Mater. 56 (2007) 1.
[54] M. Bose, S. Gayen, S.N. Behera, Phys. Rev. B 72 (2005) 153402.
[55] Y. Sato, M. Kamo, N. Setaka, Carbon 16 (1978) 279.
[56] D.W. Mayo, F.A. Miller, R.W. Hannah, Courses on the Interpretation of Infrared and Raman Spectra, Wiley-Interscience, Hoboken, NJ, 2003.
[57] J.F. Moulder, W.F. Stickle, P.E. Sobol, K.D. Bomben, in: Jill Chastain (Ed.), Handbook of X-ray Photoelectron Spectroscopy, Minnesota, 1992.
[58] S.D. Gardner, C.SK. Singamsetty, G.L. Booth, G.R. He, Carbon 33 (1995) 587.
[59] M. Seredych, E. Rodríguez-Castellón, M.J. Biggs, W. Skinner, T.J. Bandosz, Carbon 78 (2014) 540–548.
[60] N. Travlou, M. Seredych, E. Rodriguez-Castellón, T.J. Bandosz, J. Mater Chem. A 3 (2015) 3821.
[61] A. Cayuela, M.L. Soriano, M. Valcárcel, Anal. Chim. Acta 804 (2013) 246.
[62] Y. Liu, C.Y. Liu, Z.Y. Zhang, Appl. Surf. Sci. 263 (2012) 481.
[63] S.C. Hill, R.G. Pinnick, S. Niles, N.F. Fell, Y.L. Pan, J. Bottiger, B.V. Bronk, S. Holler, R.K. Chang, Appl. Opt. 40 (2001) 3005.
[64] B.K. An, S.-K. Kwon, S.-D. Jung, S. Park, J. Am. Chem. Soc. 124 (2002) 14410.
[65] U.R. Genger, M. Grabolle, S.C. Jaricot, R. Nitschke, T. Nann, Nat. Methods 5 (2008) 763.
[66] M. Jones, C. Engtrakul, W.K. Metzger, R.J. Ellingson, A.J. Nozik, M.J. Heben, G. Rumbles, Phys. Rev. B 71 (2005) 15426.
[67] K.N. Ramachandran, V.K. Gupta, Microchem. J. 44 (1991) 272.
[68] S. Amlathe, S. Upadhyay, V.K. Gupta, Microchem. J. 37 (1998) 225.
[69] Z. Li, J. Ma, Y. Zong, Y. Men, J. Alloys Comp. 559 (2013) 39.